The Shapes and Other Properties of Non-Transition Element Complexes. 2. AB_4

Benjamin M. Gimarc*[1] and Shakil A. Khan

Contribution from the Department of Chemistry, University of South Carolina, Columbia, South Carolina 29208. *Received December 1, 1976*

Abstract: A qualitative molecular orbital model of the valence electronic structure of tetrahalide complexes AB_4 is developed from the results of extended Hückel calculations on test systems. This model is used to rationalize the geometries of AB_4 complexes. Structures considered are tetrahedral, diagonally folded square (pseudo-trigonal bipyramidal), square planar, and square pyramidal. Counting all valence electrons from the central atom A and one electron from each halide ligand B, then complexes with eight valence electrons are tetrahedral, those with ten electrons have the shape of a folded square, and those with 12 electrons are square planar. Molecular orbitals for AB_4 complexes are compared with those for related AB_6 complexes. Trends in A–B bond distances and complex stabilities are discussed.

Introduction

In this paper we use a qualitative molecular orbital (MO) model of molecular electronic structure to explain, rationalize, and predict structures and other properties of non-transition element complexes of the general formula AB_4.[2] The rules of qualitative MO theory have been discussed elsewhere.[3-5]

As the AO basis for AB_4 we have chosen the single s and three p valence AOs of the central atom A and only one AO from each ligand B appropriate for the formation of a σ-type bond to the central atom. For AB_4 complexes this is a total of eight AOs from which eight MOs can be formed. The valence electrons are counted by including all of those in the valence s and p AOs of the neutral central atom plus one electron from each halogen ligand (none from oxygen or sulfur ligands) plus one electron for each negative charge on the whole complex (subtract positive charges). We have restricted our survey to those complexes in which the ligands B are individual atoms. The halogens serve as ligands in the largest set of AB_4 complexes, although there are many tetroxides and a few tetrasulfides. We have compared tetrahedral (T_d), trigonal bipyramidal (C_{2v}), square planar (D_{4h}), and square pyramidal (C_{4v}) geometries for these complexes.

Very similar qualitative MO interpretations of the shapes of AB_4 complexes have recently been published by Gleiter and Veillard[6] and by Chen and Hoffmann.[7] Gleiter and Veillard based their interpretation on their ab initio SCF MO calculations for SH_4 and SF_2H_2. Chen and Hoffmann based their study on extended Hückel calculations for SH_4. Rundle used a qualitative three-center four-electron MO model to explain the bonding in 12-electron AB_4 complexes.[8] Our work draws on extended Hückel results for a series of AH_4 test systems and the electronic structure model which we present here is a composite of those results, none of which by itself serves as a particularly good model for the whole AB_4 series. Our geometry explanations are somewhat different from but not inconsistent with those recently published.[6,7] In addition, we include Walsh diagrams[8] for tetrahedral and square pyramidal shapes and we use the qualitative orbital diagrams to compare electronic structures of related AB_4 and AB_6 complexes, and to explain the relative stabilities of complexes, bond lengths, and strengths.

Structures of AB_4 Complexes[10]

AB_4 molecules with eight valence electrons have tetrahedral (T_d) geometry. Those with ten electrons have a structure usually referred to as that of a trigonal bipyramid with one of the three equatorial valence positions vacant or, rather, occupied by a lone pair of electrons. This description is based on the positions of directed electron pairs in the five-coordinate case of the valence shell electron pair repulsion (VSEPR) model.[11] Since we are presenting an alternative model of chemical valence we introduce a different description of this C_{2v} structure, that of a square folded along one of its diagonals. We refer to the two coordinate positions on the fold axis as the axial positions and the other two positions as the equatorial positions. NMR experiments have shown that axial and equatorial ligands of SF_4 in the pure liquid undergo intramolecular exchange through a Berry pseudorotation mechanism.[12] The 12-electron AB_4 complexes are square planar (D_{4h}). Tables I, II, and III list respectively the known 8-, 10-, and 12-electron tetrahalide complexes of the representative elements in groups 3 through 0 of the periodic table. All of the known tetroxides and tetrasulfides have eight valence electrons and tetrahedral geometry. Representative examples are PO_4^{3-}, SO_4^{2-}, ClO_4^-, XeO_4,[13] SnS_4^{4-},[14] PS_4^{3-}, and SbS_4^{3-}.[15]

Some nine-electron radicals have been produced in radiation damage experiments and observed by ESR spectroscopy. Examples are PO_4^{4-},[16] AsO_4^{4-},[17] SeO_4^{3-},[18] ClO_4^{2-},[19] CBr_4^-,[20] PH_4,[21] PF_4,[22,23] PCl_4,[24] and SF_4^+.[22] These are all known or assumed to have the diagonally folded square (C_{2v}) structure of the ten-electron complexes. $POCl_3^-$ [25] and $SO_2Cl_2^-$ [26] are examples of less symmetric, mixed-ligand nine-electron radicals. These are believed to have the diagonally folded square (C_{2v}) shape with the more electronegative ligands occupying the axial positions.

The mixed-ligand ten-electron complexes also have the more electronegative ligands in the axial positions of the diagonally folded square structure.[27] Examples of this class are $ClO_2F_2^-$,[28] $IO_2F_2^-$,[29] XeO_2F_2,[30] XeO_3F^-,[31] $XeOF_3^+$,[32] and ClF_3O.[33] There is some uncertainty about the details of the axial and equatorial substitution in $TeBr_2Cl_2$.[34-37]

The 11-electron radical ClF_4 has been observed and ESR data suggest that it is square planar D_{4h}.[38]

Molecular Orbitals from Atomic Orbitals

Regular tetrahedral geometry (T_d) offers the simplest set of MOs. Starting with our eight AO basis set, the MOs of tetrahedral symmetry turn out to be two nondegenerate a_1 orbitals and two triply degenerate t_1 sets. The a_1 MOs are formed by in-phase (bonding) or out-of-phase (antibonding) combinations of the ligand AOs and the central atom s orbital. Similarly, the t_1 sets are formed by in-phase or out-of-phase combinations of ligand AOs and individual central atom p orbitals. Since the central atom s has a lower energy than the central atom p's, the bonding $1a_1$ MO will lie below the bonding $1t_1$ set in energy. The consequences for molecular shapes when only $1a_1$ and $1t_1$ are occupied by electrons have been discussed in detail elsewhere.[39] The energy order of the

0002-7863/78/1500-2340$01.00/0

Table I. AB_4 Halides—Eight Electrons

3	4	5	6	7	0
BF_4^-	CF_4	NF_4^+			
BCl_4^-	CCl_4				
BBr_4^-	CBr_4				
BI_4^-	CI_4				
AlF_4^-	SiF_4				
$AlCl_4^-$	$SiCl_4$	PCl_4^+			
$AlBr_4^-$	$SiBr_4$	PBr_4^+			
AlI_4^-	SiI_4				
GaF_4^-	GeF_4				
$GaCl_4^-$	$GeCl_4$	$AsCl_4^+$			
$GaBr_4^-$	$GeBr_4$				
GaI_4^-	GeI_4				
InF_4^-	SnF_4				
$InCl_4^-$	$SnCl_4$	$SbCl_4^+$			
$InBr_4^-$	$SnBr_4$				
InI_4^-	SnI_4				
	PbF_4				
$TlCl_4^-$	$PbCl_4$				
$TlBr_4^-$	$PbBr_4$				
TlI_4^-	PbI_4				

Table II. AB_4 Halides—Ten Electrons

3	4	5	6	7	0
		PF_4^-	SF_4	ClF_4^+	
			SCl_4		
		PBr_4^-			
		AsF_4^-	SeF_4	BrF_4^+	
		$AsCl_4^-$	$SeCl_4$		
		$AsBr_4^-$	$SeBr_4$		
		SbF_4^-	TeF_4	IF_4^+	
	$SnCl_4^{2-}$	$SbCl_4^-$	$TeCl_4$		
		$SbBr_4^-$	$TeBr_4$		
		SbI_4^-	TeI_4		
	$PbCl_4^{2-}$	$BiCl_4^-$	$PoCl_4$		
	$PbBr_4^{2-}$	$BiBr_4^-$	$PoBr_4$		
TlI_4^{3-}	PbI_4^{2-}	BiI_4^-	PoI_4		

Table III. AB_4 Halides—12 Electrons

3	4	5	6	7	0
				ClF_4^-	
				BrF_4^-	
				IF_4^-	XeF_4
				ICl_4^-	
			$PoCl_4^{2-}$		

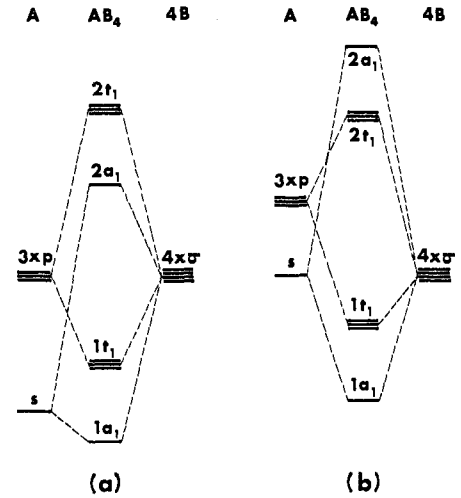

Figure 1. Correlation of MOs for tetrahedral AB_4 with AOs for separated atoms A + 4B. (a) Electronegative central atom A. (b) Electropositive A.

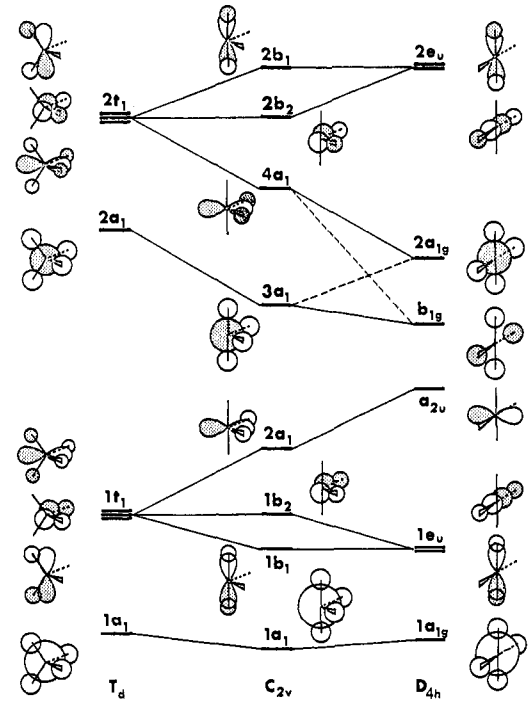

Figure 2. MO correlations for AB_4 complexes in tetrahedral (T_d), diagonally folded square (C_{2v}), and square planar (D_{4h}) shapes, assuming the ordering of tetrahedral levels from Figure 1(a).

antibonding orbitals $2a_1$ and $2t_1$ depends on further assumptions. Figure 1(a) shows the case in which the ligand AOs have energy comparable to that of the central atom p AOs, with a large energy gap between central atom s and p AOs. This arrangement would be suitable for a complex that has a rather electronegative central atom, ClF_4^+, for example. The large energy gap between central atom s and p AOs and the small perturbation interaction between ligand AOs and the central atom s combine to make $2a_1$ fall below $2t_1$. In Figure 1(b) the ligand AO energy is near that of the central atom s orbital and there is a small energy gap between central atom s and p orbitals, an alignment that should be more appropriate for a complex such as AlF_4^-, in which the central atom is considerably less electronegative than the ligands. Here the small energy gap between the central atom s and p and the strong perturbation interaction between the central atom s and the ligand AOs combine to push $2a_1$ above $2t_1$.

Figure 2 correlates orbital energy levels for AB_4 complexes through successive angular rearrangements from regular tetrahedral (T_d) through diagonally folded square (C_{2v}) to square planar (D_{4h}) geometries. In this and following diagrams we assume that all A–B bond lengths remain equal and constant through changes in angular geometry. The order of energy levels chosen for tetrahedral geometry is that for an electronegative central atom, Figure 1(a). Changes in orbital energy from shape to shape follow changes in AO overlap. The contributions of AOs on the axial ligands in $2a_1$ and $4a_1$ (C_{2v}) need not be zero but since they are near nodal surfaces one would expect them to be small and hence they are omitted in Figure 2.

Consider the $2a_1$ (T_d)–$3a_1$ (C_{2v}) orbital. Opening a tetrahedral angle produces no overlap changes between the ligand AOs and the central atom s AO, but there are overlap changes

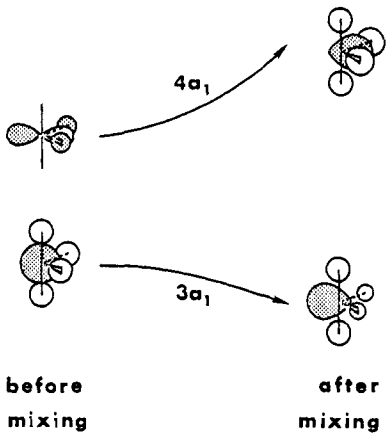

Figure 3. Orbital mixing gives more realistic representations of MOs for C_{2v} geometry.

among the ligand orbitals themselves. Although these overlaps are rather small because of the relatively long ligand–ligand distances, the overlap changes are amplified by the fact that the ligand AO coefficients in $2a_1$ (T_d) are large owing to the large number of phase differences within that MO.[4] Opening a tetrahedral angle to diagonally folded square geometry moves ligands closer together, increasing the in-phase overlaps among ligand orbitals and lowering the energy of $3a_1$ (C_{2v}) relative to that of $2a_1$ (T_d). In tetrahedral geometry $2a_1$ (T_d) has six ligand–ligand overlaps that are 109.5° apart. In folded square geometry $3a_1$ (C_{2v}) has four ligand–ligand overlaps that have closed to 90° apart, one set still at 109.5°, and one set that has opened to 180°. Moving on from diagonally folded square to square planar (D_{4h}) shape only one angle changes and one ligand–ligand overlap decreases when its angle opens from 109.5° to 180°. The other five angles and overlaps remain constant. Therefore, the energy should increase from $3a_1$ (C_{2v}) to $2a_{1g}$ (D_{4h}) and this intended correlation is indicated by a dashed connecting line in Figure 2.

The orbitals $1t_1$–$2a_1$–a_{2u} and $2t_1$–$4a_1$–b_{1g} require special examination. As the tetrahedron flattens to the plane the ligand orbitals move from good overlap positions in $1t_1$ (T_d) to the nodal plane of the central atom p orbital in a_{2u} (D_{4h}), leaving a_{2u} (D_{4h}) as a free central atom p or nonbonding MO. The same process might appear to proceed in the higher energy $2t_1$–$4a_1$–b_{1g} case. Here, out-of-phase interactions are reduced as ligand AOs move away from the lobes of the central atom p orbital and toward the nodal surface of the central atom p, as in $4a_1$ (C_{2v}). However, further flattening cannot cause the ligand AO contributions to vanish from this MO because that would reproduce the a_{2u} (D_{4h}) orbital we already have at lower energy. Instead, the central atom p vanishes leaving b_{1g} (D_{4h}) as four ligand AOs of alternate phase, just as they were in the $2t_1$ component from which this MO originated. A dashed tie line in Figure 2 shows the intended correlation of $4a_1$ (C_{2v}) and b_{1g} (D_{4h}). On the energy scale we have placed the nonbonding b_{1g} orbital below the antibonding $2a_{1g}$ (D_{4h}) MO, although with a small central atom and large ligands, ligand–ligand out-of-phase overlaps might make b_{1g} antibonding. We assumed that we were studying a system with a rather electronegative central atom. Therefore, we feel justified in placing the central atom pure p nonbonding a_{2u} MO below the nonbonding b_{1g} MO that contains ligand–ligand antibonding interactions. Notice that b_{1g} and $2a_{1g}$ (D_{4h}) would both be classified as a_1 under C_{2v} symmetry. Since orbitals of the same symmetry cannot cross, the intended correlations $3a_1$ (C_{2v})–$2a_{1g}$ (D_{4h}) and $4a_1$ (C_{2v})–b_{1g} (D_{4h}) are not allowed. Instead, the actual connections are those shown with solid lines in Figure 2.

The noncrossing of intended correlations between C_{2v} and D_{4h} MOs does introduce some uncertainty about where $2a_{1g}$ (D_{4h}) lies on the energy ladder relative to $4a_1$ (C_{2v}) and how b_{1g} (D_{4h}) compares with $3a_1$ (C_{2v}). Overlap arguments put $2a_{1g}$ (D_{4h}) below $2a_1$ (T_d) and therefore probably well below $4a_1$ (C_{2v}) also. Overlap arguments also place $3a_1$ (C_{2v}) below $2a_{1g}$ (D_{4h}), and therefore the antibonding $3a_1$ (C_{2v}) orbital might have an energy that is comparable to or not much higher than nonbonding b_{1g} (D_{4h}). Since $2a_1$ (T_d)–$3a_1$ (C_{2v})–b_{1g} (D_{4h}) is the highest occupied MO in ten-electron AB_4 complexes, the size of the energy difference between $3a_1$ (C_{2v}) and b_{1g} (D_{4h}) is crucial to structural conclusions for these complexes. If $3a_1$ is too high, the energy drop from $3a_1$ to b_{1g} will overcome the energy rise of the lower occupied $2a_1$ (C_{2v})–a_{2u} (D_{4h}) system and the model will predict that ten-electron AB_4 complexes should be square planar, contrary to observation. This difficulty has troubled previous similar models.[6,7] In our model we have assumed central atom and ligand relative AO energies as shown in Figure 1(a), placing $2a_1$ below $2t_1$ for tetrahedral geometry. This means that $3a_1$ (C_{2v}) will be even lower in energy than $2a_1$ (T_d) and, in particular, lower than the $4a_1$ (C_{2v}) orbital from which b_{1g} (D_{4h}) originates.

Orbital mixing provides still another argument for a relatively low energy for $3a_1$ (C_{2v}) and it gives more realistic representations of the C_{2v} MOs. Some of the C_{2v} MOs, produced through distortions of the orbitals of the higher symmetry T_d or D_{4h} structures, do not contain all of the AOs that the lower symmetry permits. For example, symmetry does not require the absence of a horizontal p orbital on the central atom in $3a_1$ (C_{2v}) as it does for the related orbitals $2a_1$ (T_d) and $2a_{1g}$ (D_{4h}). Similarly, a central atom s orbital could enter $4a_1$ (C_{2v}) but not the related $2t_1$ (T_d) component or b_{1g} (D_{4h}). Our orbital mixing rule requires the mixing of the highest energy pair of MOs of a given symmetry classification if the two MOs are composed of different kinds of AOs. This rule clearly applies to the $3a_1$ and $4a_1$ orbitals of the diagonally folded square shape and Figure 3 shows their mixing. The after-mixing form of $3a_1$ is the sum $3a_1 + 4a_1$ of the unmixed MO pictures of Figure 2, while the after-mixing version of $4a_1$ is the difference $3a_1 - 4a_1$. After mixing, the $3a_1$ MO, with a large lobe pointing electron density away from the vertex of the two equatorial ligand bonds, looks much like the nonbonding lone pair orbital of the VSEPR model. Mixing stabilizes $3a_1$.

The correlation diagram of Figure 2 is now ready to be considered as a whole. For eight-electron complexes the bonding $1t_1$ (T_d) MOs are fully occupied and higher energy orbitals are empty. Angular changes to C_{2v} or D_{4h} shapes lead to a considerable total energy increase; therefore, the eight-electron complexes are tetrahedral. For ten-electron complexes the highest occupied orbital system is $2a_1$ (T_d)–$3a_1$ (C_{2v})–b_{1g} (D_{4h}). The large energy drop from $2a_1$ (T_d) to $3a_1$ (C_{2v}) outweighs the increase from $1t_1$ (T_d) to $2a_1$ (C_{2v}) below and gives the ten-electron complexes the diagonally folded square structure. The drop must be steep enough to give the nine-electron radicals the C_{2v} structure as well. We have argued that the slope downward from $3a_1$ (C_{2v}) is a modest one. Therefore, at least by itself, it is not enough to overcome the rising $2a_1$ (C_{2v})–a_{2u} (D_{4h}) level below and ten-electron complexes are held at the diagonally folded square structure. The square planar structure must not be too much higher in energy, however. The fact that SF_4 undergoes axial–equatorial ligand exchange at room temperatures[27] means that square planar geometry must be only a few kcal/mol higher than the folded square structure. Finally, in 12-electron complexes the orbital system $2t_1$ (T_d)–$4a_1$ (C_{2v})–$2a_{1g}$ (D_{4h}) is occupied. The energy drop across this system makes 11- and 12-electron complexes rigidly square planar.

Had we constructed Figure 2 assuming the energy level ordering of Figure 1(b), the relative order of orbitals labeled

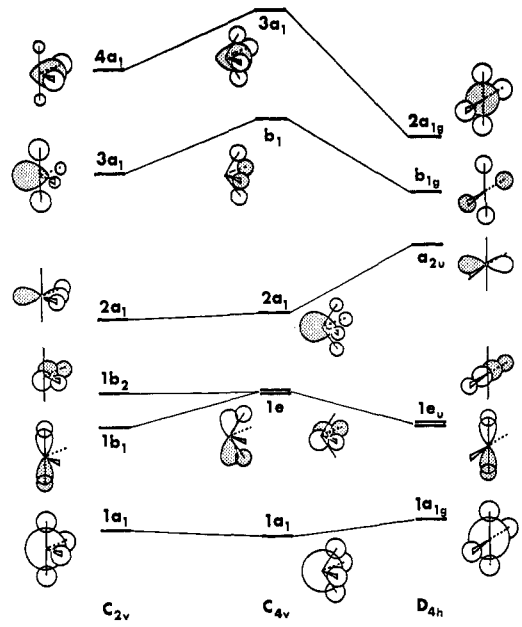

Figure 4. MO correlations for AB_4 complexes in diagonally folded square (C_{2v}), square pyramidal (C_{4v}), and square planar shapes (D_{4h}).

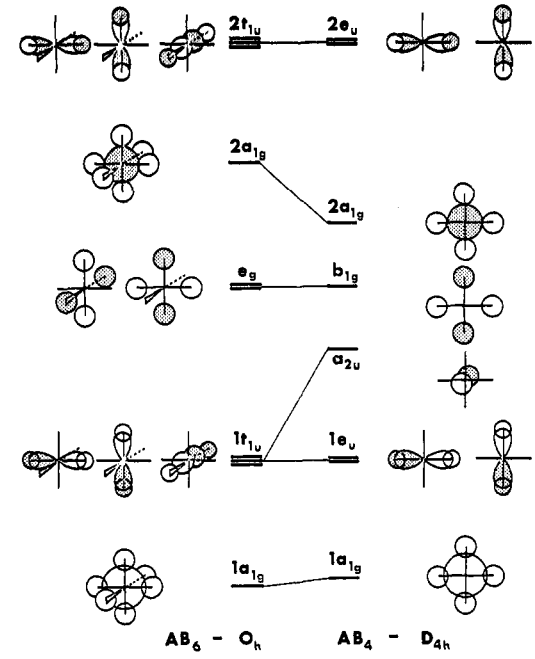

Figure 5. Comparison of octahedral (O_h) AB_6 MOs with MOs for square planar AB_4.

$3a_1$ and $4a_1$ in Figure 2 would have been reversed, producing a continuous and steep energy decline from $2t_1$ (T_d) to $3a_1$ (C_{2v}) to b_{1g} (D_{4h}) and leading to square planar geometry complexes.

Another structure that has been considered for four-coordinate complexes is the square pyramid (C_{4v}). Figure 4 correlates MOs of square pyramidal geometry with those for diagonally folded square and square planar shapes. There are three orbitals of a_1 symmetry for C_{4v} and we have already mixed the two of highest energy, $2a_1$ and $3a_1$ (C_{4v}), for representation in Figure 4. They are very similar to the related C_{2v} orbitals in Figure 3. The system $2a_1$ (C_{2v})-$2a_1$ (C_{4v})-a_{2u} (D_{4h}) is the highest occupied orbital for eight-electron complexes and in Figure 4 the energy slope of this MO system suggests that square pyramidal or diagonally folded square carbon might be more easily achievable goals for those synthetic chemists who seek alternatives to tetrahedral geometry for tetracoordinate carbon, a conclusion supported by the results of recent ab initio calculations.[40] For ten electrons, the highest occupied MO system is $3a_1$ (C_{2v})-b_1 (C_{4v})-b_{1g} (D_{4h}). The AO compositions of b_1 (C_{4v}) and $3a_1$ (C_{2v}) are quite different, but symmetry requires that they be connected since b_1 is classified as a_1 under C_{2v} symmetry. Clearly, C_{4v} geometry, with the close association of four ligand AOs of alternate phase in b_1 (C_{4v}), is a high-energy structure for ten-electron complexes. For 12 electrons the $4a_1$ (C_{2v})-$3a_1$ (C_{4v})-$2a_{1g}$ (D_{4h}) system is filled. The orbital $3a_1$ (C_{4v}) is higher in energy than $2a_{1g}$ (D_{4h}) because $3a_1$ has its ligand AOs pushing into a big central lobe of opposite phase. The energies of $3a_1$ (C_{4v}) and $4a_1$ (C_{2v}) may be comparable. In $4a_1$ (C_{2v}) the equatorial ligand AOs are large contributors and they are very close to a large central lobe of opposite phase. As the axial ligands fold toward each other to form the square pyramid, the equatorial ligand AO coefficients shrink and the axial AO coefficients grow. In $3a_1$ (C_{4v}) contributions from all four ligand AOs are equal. It is clear that the square pyramidal structure is high in energy compared to the folded square and square planar shapes.

Other Properties of the Folded Square Structure

Reconsider for a moment the $3a_1$ MO of folded square geometry after mixing as shown in Figure 3. Closing the equatorial angle to less than the tetrahedral value would increase overlaps in both $2a_1$ and $3a_1$ (C_{2v}), leading to slightly lower energy. Table IV shows that the equatorial angles of SF_4[41] and SeF_4[42] are both less than 109.5°. Notice that orbital mixing has reduced the contributions from the equatorial ligand AOs in $3a_1$, reducing the electron density in the equatorial positions relative to that in the axial positions. Therefore, in complexes with mixed ligands such as XeO_2F_2 the more electronegative ligands should prefer axial positions where they can receive the extra electron density. This is in accord with the observation that the more electronegative ligands do occupy axial sites in mixed-ligand ten-electron complexes.[27] The larger axial coefficients in $3a_1$ give a larger antibonding contribution to the $A-B_{ax}$ bond order than the smaller equatorial coefficients do to the $A-B_{eq}$ bond order, making the axial bonds longer and weaker than the equatorial bonds. The structural data in Table IV show that this is the case. Finally, if the axial ligands could lean away from the central atom lobe in $3a_1$, out-of-phase overlaps could be reduced. Again, the structural data in Table IV show that the axial ligands do lean slightly toward the equatorial ligands. (Apparently, the axial fluorines in XeO_2F_2 lean away from the equatorial oxygens.)[30]

Table IV. Bond Distances and Angles for 10-Electron AB_4 and 12-Electron AB_6 Complexes

	SF_4[a]	SF_6[b]	SeF_4[c]	SeF_6[b]
$r(A-B_{ax})$, Å	1.646		1.771	
$r(A-B_{eq})$, Å	1.545		1.682	
$r(A-B)_{av}$, Å	1.596	1.564	1.727	1.688
$\angle B_{eq}-A-B_{eq}$	101.55°		100.55°	
$\angle B_{ax}-A-B_{ax}$	173.07°		169.20°	

[a] Reference 41. [b] V. C. Ewing and L. E. Sutton, *Trans. Faraday Soc.*, **59**, 1241 (1963). [c] Reference 42.

Comparison of MOs for AB_4 and AB_6

Figure 5 compares MOs for AB_6 complexes in octahedral (O_h) geometry and AB_4 complexes of square planar (D_{4h}) shape. Each square planar AB_4 complex has 12 valence electrons. An octahedral AB_6 complex in which the related MOs are occupied has 14 electrons. For all but one of the six known 12-electron AB_4 complexes the corresponding 14-electron AB_6 complex exists. Examples are BrF_4^- and BrF_6^-. The AB_4

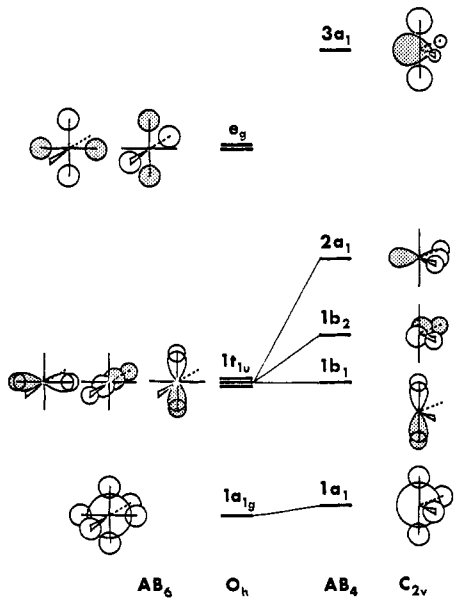

Figure 6. Comparison of octahedral AB_6 MOs with those for diagonally folded square AB_4.

system has one less nonbonding MO, one of the e_g (AB_6) pair being missing. Only those AB_4 (12e, D_{4h}) complexes composed of the most electronegative elements exist. The approximate cancellation of four pairs of ligand–ligand in-phase interactions in $2a_{1g}$ by an equal number of ligand–ligand out-of-phase interactions in b_{1g} (D_{4h}) nearly eliminates the 12-electron AB_4 series and reduces the resemblence of this series to the 14-electron AB_6 complexes.

The $2a_{1g}$ MO of AB_6 is sometimes described as containing an electron pair that is possibly stereochemically active[43] because in some cases (XeF_6 being the noted example) it is responsible for distortions of the geometry from octahedral symmetry.[4] The $2a_{1g}$ (AB_6) has an energy maximum in octahedral geometry. The distortions are a result of the 12 in-phase ligand–ligand overlaps in $2a_{1g}$ (AB_6). The corresponding $2a_{1g}$ MO of square planar AB_4 is not noted for stereochemical activity because it has only four ligand–ligand overlaps. An orbital of the AO composition of $2a_{1g}$ (AB_4) has maximum energy in tetrahedral geometry as $2a_1$ (T_d).

There is a remarkable similarity among the occupied MOs for 14-electron octahedral AB_6, 12-electron square planar AB_4, and 10-electron linear AB_2 complexes. Because of this orbital relationship one might expect the A–B bond distances to be equal through a series composed of the same kinds of atoms. Excellent data are available for the xenon fluorides. Compare the Xe–F distances in XeF_6 (1.890 ± 0.005 Å, gas-phase electron diffraction),[44] in XeF_4 (1.951 and 1.954 ± 0.002 Å, neutron diffraction in crystal),[45] and in XeF_2 (1.977 ± 0.002 Å, high-resolution gas-phase infrared spectrum).[46] The complexes are not in the same phase and the experimental methods are all different, but the differences in bond distances are over ten times the stated uncertainties in the results. We believe that we can account for the trend in bond distances on the basis of differences in A–B antibonding interactions between $2a_{1g}$ (AB_6), $2a_{1g}$ (AB_4), and $2\sigma_g$ (AB_2), the highest occupied MOs of these complexes. Because there are fewer ligands in AB_4 than in AB_6, MO normalization requires that ligand AO coefficients be larger in $2a_{1g}$ (AB_4) than in $2a_{1g}$ (AB_6). The ligand coefficients in $2\sigma_g$ (AB_2) should be still larger. Therefore, individual bond order contributions (proportional to the product of central atom and ligand AO coefficients) should increase in magnitude from XeF_6 to XeF_4 to XeF_2. Since these contributions are antibonding in each of these MOs the increase in magnitude weakens the A–B bond so that bond lengths should increase from XeF_6 to XeF_4 to XeF_2 as observed. We predict similar trends in the following series of known complexes for which bond distances have not been measured. Triplets, ClF_6^-, ClF_4^-, ClF_2^-; BrF_6^-, BrF_4^-, BrF_2^-; pairs, IF_6^-, IF_4^-; $PoCl_6^{2-}$, $PoCl_4^{2-}$.

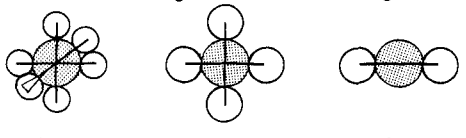

Figure 6 shows the relationship between the six occupied MOs of octahedral AB_6 and the five occupied MOs of an AB_4 complex in diagonally folded square geometry (assuming a 90° angle between equatorial ligands). Unlike the O_h–D_{4h} comparison, the O_h–C_{2v} MO systems are quite different. Only one orbital, $1t_{1u}$ (O_h)–$1b_1$ (C_{2v}), is identical in both. Poorer overlaps make $1b_2$ and $2a_1$ (C_{2v}) individually weaker bonding orbitals than related orbitals in $1t_{1u}$ (O_h) but this does not necessarily make the equatorial bonds in AB_4 weaker than bonds in AB_6. Both $2a_1$ and $1b_2$ (C_{2v}) are A–B_{eq} bonding while each $1t_{1u}$ (O_h) component bonds a different pair of ligands. To put it another way, the bond orbitals that are produced by the sum and difference of $2a_1$ and $1b_2$ (C_{2v}) are comparable in bond order to individual members of $1t_{1u}$ (O_h). Finally, the AB_4 complexes have an axial antibonding, equatorial nonbonding MO, $3a_1$ (C_{2v}), while the AB_6 complexes have a pair of nonbonding MOs, e_g (O_h). Table IV contains bond distances for the pairs SF_4, SF_6 and SeF_4, SeF_6. The equatorial AB distances of the AB_4 complexes are very close to the A–B distances in the comparable AB_6 complexes. The axial A–B distances in AB_4 are longer.

Comparing Tables I and II one finds eight pairs of isoatomic AB_4 complexes such as PBr_4^+ and PBr_4^-, each pair consisting of an eight-electron complex and a ten-electron complex composed of the same number and kinds of atoms but with the central atoms differing by 2 in oxidation states. The additional electron pair in the ten-electron series occupies the A–B antibonding $3a_1$ (C_{2v}) MO. Therefore, the ten-electron complexes should have longer A–B bonds than the isoatomic eight-electron complexes. Unfortunately, no bond distances have been reported for the ten-electron complexes in the known isoatomic pairs.

Relative Stabilities of AB_4 Complexes

The ten-electron AB_4 complexes listed in Table II fill out nearly the same portions of the periodic table as do the 14-electron AB_6 complexes.[4] From among 32 complexes in the ten-electron series and 30 complexes in the 14-electron AB_6 series, there are 23 related pairs such as $SeBr_4$, $SeBr_6^{2-}$. The highest occupied MO in the ten-electron AB_4 complexes is $3a_1$ (C_{2v}). In its unmixed form, $3a_1$ (AB_4, C_{2v}) is related to $2a_{1g}$ (AB_6, O_h). The in-phase overlaps among cis ligand AOs in $2a_{1g}$ (AB_6, O_h) explain the preferred stability of large ligand complexes (iodides over bromides, etc.) in the 14-electron AB_6 series,[4] contrary to what one would expect on the basis of ligand repulsion arguments from conventional valence theory. (Note as exceptions those complexes in which the central atom is unusually electronegative, i.e., the halogens and the rare gases.) In-phase ligand–ligand overlaps are also present in $3a_1$ (AB_4, C_{2v}) and could give rise to a similar preferred order of stabilities in the ten-electron AB_4 series. However, the in-phase overlaps must be considerably less effective in the AB_4 series than they are in the AB_6 complexes because the smaller number of ligands reduces the number of overlap pairs from 12 in AB_6 (O_h) to 5 in AB_4 (C_{2v}). But, other things not intervening and with the exception noted concerning strongly electronegative central atoms, the iodides are preferred for the ten-electron AB_4 series. Other chemical evidence supports this

trend. For example, emf and solubility studies of the tetrahalide complexes of BiX_4^- and TlX_4^{3-} have been interpreted as demonstrating the increasing strength of those complexes in the order Cl < Br < I.[47,48]

In the 12-electron AB_4 complexes the highest occupied MO is still the antibonding $2a_{1g}$ (D_{4h}) which is related through AO composition to $3a_1$ (C_{2v}) and to $2a_{1g}$ (AB_6, O_h). As we shift from the ten-electron AB_4 series to the 12-electron series, the added electron pair goes into the nonbonding b_{1g} (D_{4h}) MO that lies below $2a_{1g}$ (D_{4h}). See Figure 2. The related e_g MOs of AB_6 complexes determine the stabilities of the 12-electron AB_6 complexes. In that series, fluorides of large central atoms predominate. The b_{1g} orbitals of AB_4 are also stabilized by small ligands and large central atoms that reduce the four pairs of out-of-phase ligand–ligand overlaps that occur in b_{1g}. The four pairs of in-phase ligand–ligand overlaps in $2a_{1g}$ (D_{4h}) favor large ligand complexes. In the 12-electron AB_4 complexes, the opposing effects of b_{1g} and $2a_{1g}$ (D_{4h}) approximately cancel, nearly eliminating the whole series. Table III contains only six known 12-electron AB_4 complexes compared to 30 in the 14-electron AB_6 series in which the highest occupied MO contains 12 pairs of in-phase ligand–ligand overlaps.

Summary

By qualitatively comparing the MO energies of AB_4 complexes in tetrahedral (T_d), diagonally folded square (C_{2v}), square planar (D_{4h}), and square pyramidal (C_{4v}) shapes, one can understand why eight-electron complexes are tetrahedral, ten-electron complexes have diagonally folded square shapes, and 12-electron complexes are square planar. The preference of more electronegative ligands for axial positions in mixed ligand AB_4 complexes of diagonally folded square shape is apparent from the AO composition of the highest occupied MO as a result of MO mixing. MO normalization limits the size of AO coefficients in the highest occupied MOs of AB_6 (14e, O_h), AB_4 (12e, D_{4h}), and AB_2 (10e, $D_{\infty h}$) and explains a trend in increasing bond distances through the series XeF_6, XeF_4, and XeF_2. Ligand–ligand overlaps in the highest occupied MOs of AB_4 (10e, C_{2v}) and AB_6 (14e, O_h) explain the observation that these two series of complexes are composed of the same elements and have similar trends in stabilities (B = $Cl^- < Br^- < I^-$). Despite the fact that the highest occupied MO of AB_4 (12e, D_{4h}) complexes is closely related to the highest occupied orbital in AB_6 (14e, O_h), these two series have different compositions and stabilities which can be understood on the basis of numbers of ligand–ligand AO interactions in the higher occupied MOs. Qualitative MO theory can serve as the conceptual framework for a large part of inorganic chemistry.

Acknowledgment. The research was sponsored by a grant from the National Science Foundation.

References and Notes

(1) To whom correspondence should be addressed.
(2) A preliminary version of this paper was presented at the 27th Southeastern–31st Southwestern Regional Meeting of the American Chemical Society, Memphis, Tenn., Oct 29–31, 1975, Paper No. 286.
(3) B. M. Gimarc, *Acc. Chem. Res.*, **7**, 384 (1974).
(4) B. M. Gimarc, J. F. Liebman, and M. Kohn, preceding paper in this issue.
(5) J. P. Lowe, *J. Am. Chem. Soc.*, **98**, 3759 (1974).
(6) R. Gleiter and A. Veillard, *Chem. Phys. Lett.*, **37**, 33 (1976).
(7) M. M. L. Chen and R. Hoffmann, *J. Am. Chem. Soc.*, **98**, 1647 (1976).
(8) R. E. Rundle, *J. Am. Chem. Soc.*, **85**, 112 (1963).
(9) A. D. Walsh, *J. Chem. Soc.*, 2260 (1953), and papers immediately following.
(10) Representative structural data may be found in L. E. Sutton, Ed., *Chem. Soc., Spec. Publ.*, **No. 11** (1958); **No. 18** (1965).
(11) R. J. Gillespie and R. S. Nyholm, *Q. Rev., Chem. Soc.*, **11**, 339 (1957); R. J. Gillespie, *J. Chem. Educ.*, **47**, 18 (1970); **51**, 367 (1974).
(12) W. G. Klemperer, J. K. Krieger, M. D. McCreary, E. L. Muetterties, D. D. Traficante, and G. M. Whitesides, *J. Am. Chem. Soc.*, **97**, 7023 (1975).
(13) G. Gundersen, K. Hedberg, and J. L. Huston, *J. Chem. Phys.*, **52**, 812 (1970).
(14) S. Ichiba, M. Katada, and H. Negita, *J. Inorg. Nucl. Chem.*, **37**, 2249 (1975).
(15) A. Müller, E. Diemann, and M. J. Leroy, *Z. Anorg. Allg. Chem.*, **372**, 113 (1970).
(16) M. C. R. Symons, *J. Chem. Phys.*, **53**, 857 (1970).
(17) M. Hampton, F. G. Herring, W. C. Lin, and C. A. McDowell, *Mol. Phys.*, **10**, 565 (1966).
(18) K. V. S. Rao and M. C. R. Symons, *J. Chem. Soc., Dalton Trans.*, *147 (1972)*.
(19) M. B. D. Bloom, R. S. Eachus, and M. C. R. Symons, *J. Chem. Soc. A*, 1235 (1970).
(20) S. P. Mishra and M. C. R. Symons, *J. Chem. Soc., Chem. Commun.*, 577 (1973).
(21) A. J. Colussi, J. R. Morton, and K. F. Preston, *J. Chem. Phys.*, **82**, 2004 (1975).
(22) R. W. Fessenden and R. H. Schuler, *J. Chem. Phys.*, **45**, 1845 (1966).
(23) W. Nelson, G. Jackel, and W. Gordy, *J. Chem. Phys.*, **52**, 4572 (1970).
(24) G. F. Kokoszka and F. E. Brinckman, *J. Am. Chem. Soc.*, **92**, 1199 (1970); S. P. Mishra and M. C. R. Symons, *J. Chem. Soc., Dalton Trans.*, 139 (1976).
(25) A. Begum and M. C. R. Symons, *J. Chem. Soc. A*, 2065 (1971).
(26) T. Gillbro and F. Williams, *Chem. Phys. Lett.*, **20**, 436 (1973); K. V. S. Rao and M. C. R. Symons, *J. Chem. Soc., Dalton Trans.*, 9 (1973).
(27) E. L. Muetterties and R. A. Schunn, *Q. Rev., Chem. Soc.*, **20**, 245 (1966).
(28) K. O. Christe and E. C. Curtis, *Inorg. Chem.*, **11**, 35 (1972).
(29) L. Helmholz and M. T. Rogers, *J. Am. Chem. Soc.*, **62**, 1537 (1940).
(30) H. H. Claassen, E. L. Gasner, H. Kim, and J. L. Huston, *J. Chem. Phys.*, **49**, 253 (1968); S. W. Peterson, R. D. Willett, and J. L. Huston, *ibid.*, **59**, 453 (1973).
(31) D. J. Hodgson and J. A. Ibers, *Inorg. Chem.*, **8**, 326 (1969).
(32) D. E. McKee, C. J. Adams, A. Zalkin, and N. Bartlett, *J. Chem. Soc., Chem. Commun.*, 26 (1973).
(33) K. O. Christe and E. C. Curtis, *Inorg. Chem.*, **11**, 2196 (1972).
(34) N. Katsaros and J. W. George, *Inorg. Chim. Acta*, **3**, 165 (1969).
(35) G. A. Ozin and A. Vander Voet, *Chem. Commun.*, 1489 (1970); *Can. J. Chem.*, **49**, 704 (1971).
(36) G. A. Ozin and A. Vander Voet, *J. Mol. Struct.*, **10**, 397 (1971).
(37) I. R. Beattie, O. Bizri, H. E. Blayden, S. C. Brumbach, A. Bukovszky, T. R. Gilson, R. Moss, and B. A. Phillips, *J. Chem. Soc., Dalton Trans.*, 1747 (1974).
(38) J. R. Morton and K. F. Preston, *J. Chem. Phys.*, **58**, 3112 (1973).
(39) B. M. Gimarc, *J. Am. Chem. Soc.*, **93**, 593 (1971).
(40) V. I. Minkin, R. M. Minyaev, and I. I. Zacharov, *J. Chem. Soc., Chem. Commun.*, 213 (1977).
(41) W. M. Tolles and W. D. Gwinn, *J. Chem. Phys.*, **36**, 1119 (1962).
(42) I. C. Bowater, R. D. Brown, and F. R. Burden, *J. Mol. Spectrosc.*, **28**, 454 (1968).
(43) D. S. Urch, *J. Chem. Soc.*, 5775 (1964).
(44) R. M. Gavin and L. S. Bartell, *J. Chem. Phys.*, **48**, 2460 (1968).
(45) J. H. Burns, P. A. Agron, and H. A. Levy, *Science*, **139**, 1208 (1963).
(46) S. Reichman and F. Schreiner, *J. Chem. Phys.*, **51**, 2355 (1969).
(47) S. Ahrland and I. Grenthe, *Acta Chem. Scand.*, **11**, 1111 (1957).
(48) R. O. Nilsson, *Ark. Kemi*, **10**, 363 (1957).